JASA EXPRESS LETTERS ARTICLE asa.scitation.org/journal/jel

Extraction of the direct scattering of a sphere in a vortex beam: Theory and experiment

Liwei Chen,[1,a] Jun Fan,[1,2,b] and Zhixiong Gong[1,2,c]
[1]State Key Laboratory of Ocean Engineering, School of Ocean and Civil Engineering, Shanghai Jiao Tong University, Shanghai, 200240, China
[2]Key Laboratory of Marine Intelligent Equipment and System, Ministry of Education, Shanghai, China

Abstract: The suppression of direct forward scattering is challenging for object detection in the underwater environment under the incidence of quasi-planar waves. In this work, we study the lateral spatial phase of forward acoustic scattering in a vortex beam from a sphere. By subtracting a stable incident contribution, the forward scattering is extracted from the total field with good agreement between our experimental measurements and numerical simulations. A cross correlation method of the spatial phase is proposed, and results show a linear dependence of the phase singularity shift versus the sphere's offset to the beam axis, which may be potential for the underwater target detection and positioning by using the spatial phase information as the degree of freedom.

[Editor: T. Douglas Mast] https://doi.org/10.1121/10.0043233

Received: 9 February 2026 **Accepted:** 20 March 2026 **Published Online:** 3 April 2026

1. Introduction

Since Bessel beams were first derived by Durnin and co-workers,[1,2] this unique class of acoustic fields has attracted extensive attention and has been extended to the Bessel vortex[3,4] with orbital angular momentum, particularly in areas such as particle manipulation[5,6] and communication.[7,8] While these applications often exploit the amplitude profile of the beam, the spatial phase structure holds considerable potential but remains relatively underexplored. Characterized by a topological charge (or order) M, the phase varies azimuthally as $e^{iM\varphi}$ with φ the cylindrical azimuthal angle. For helical wavefronts ($M \neq 0$), a central singularity forms on the beam axis and is surrounded by regions of large phase gradient described as the phase superoscillation. Research on the phase properties of vortex beams suggests promising potential for underwater alignment,[9,10] imaging,[11,12] and detection.[10,13]

It is well known that the acoustic scattering of an object from vortex beams has been well studied in theory. For ideal Bessel beams and vortexes, the analytical solutions for scattering by on-axis and arbitrarily positioned spherical targets were given by Marston[3,14] and Gong *et al.*,[4] respectively. For arbitrary beams, Baresch *et al.*[15] derived the scattering solution for a spherical target based on the multipole expansion method with the spherical basis centered on the sphere. Sapozhnikov and Bailey[16] introduced a general method based on the angular spectrum method (ASM), which decomposes an arbitrary acoustic field into plane waves and numerically solves the scattering problem under realistic illumination conditions. The above methods are demonstrated equivalent by Gong and Baudoin.[6] In addition, other methods such as the T-matrix[17,18] and the finite element method[19] are also implemented for the scattering from complex targets in vortex beam. In contrast, experimental studies on the scattering of vortex beams remain relatively limited.[9,10,20] It is worth noting that a diffraction experiment of vortex beams has been conducted from a hole in a metal plate immersed in water and demonstrated the sub-wavelength resolution for acoustic imaging.[11] This is the motivation for us to develop the scattering model and experiment setup of a sphere from a vortex beam which may be potential to use low-frequency (i.e., large wavelength) waves to detect small-sized targets. A new challenge occurs that the forward scattering contribution is weak compared with the direct incident wave in our proposed configuration which is also a bottleneck problem in the field of underwater acoustics with quasiplanar waves. This is not tackled in the pioneer work by Brunet *et al.*[11] since the separation procedure of the pure scattering contribution from the total scattering is not necessary. In this work, we provide a possibility to solve this issue by subtracting the incident background from the total measured acoustic field with the assumption that the incident background field is stable.

[a)]Email: kraken1895@sjtu.edu.cn
[b)]Email: fanjun@sjtu.edu.cn
[c)]Corresponding author: zhixiong.gong@sjtu.edu.cn

In our stable and controlled laboratory watertank environment equipped with three-axis scanning motor steppers of 1-μm step size from the Precision Acoustics, Ltd., the relative phase between the direct incident and scattered waves remains nearly constant over time. This would also be efficient in field experiments if the above assumption is met for possible dynamic measurements with and without targets and in a relatively short distance. Hence, the scattering contribution in experiments can be isolated from the total (i.e., incident and pure scattering) field with a target by directly subtracting a pre-measured background signal without the target.[21] Based on this approach, the present work demonstrates the feasibility to use the spatial phase information of the scattering from a sphere in a vortex beam both numerically and experimentally. We simulated and measured the pressure field disturbances of acoustic scattering from a solid polymethyl methacrylate (PMMA) sphere located either on or off the beam axis of a vortex beam with emphasis on the lateral spatial phase in the forward direction. The results reveal the linear dependence of the spatial phase singularity with respect to the offset of the sphere off the beam axis, which shows the potential of vortex beams for underwater target detection and positioning with a new configuration.

2. Simulation of acoustic scattering from realistic vortex beams

To understand the acoustic scattering of a finite-aperture vortex beam used in our experiment, the ASM is employed. Assuming that the frequency is f and the angular frequency $\omega = 2\pi f$ (omitting the time-dependence factor $e^{-i\omega t}$ throughout), the incident pressure $p_i(x, y, z)$ can be expressed as a superposition of plane waves via the spatial Fourier transform[16,22]

$$p_i(x,y,z) = \frac{1}{4\pi^2}\int\int_{k_x^2+k_y^2\le k^2} S(k_x,k_y)|_{z=0} e^{ik_x x + ik_y y + ik_z z} dk_x dk_y, \tag{1}$$

where $k_z = \sqrt{(k^2 - k_x^2 - k_y^2)}$ for a monochromatic wave with the wavenumber k and $S(k_x, k_y)|_{z=0}$ is the angular spectrum at the source plane ($z = 0$)

$$S(k_x,k_y)|_{z=0} = \int_{-\infty}^{+\infty}\int_{-\infty}^{+\infty} p_i(x,y,z=0) e^{-ik_x x - ik_y y} dxdy. \tag{2}$$

The integration region is confined to $k_x^2 + k_y^2 \le k^2$ since the plane wave turns into an evanescent wave decreasing rapidly beyond this region. Therefore, the total scattering of an arbitrary field by a sphere can be calculated by summing the scattered contributions from each constituent plane wave. In the spherical coordinate system (r, θ, φ), the beam vector is expressed as (k, θ_k, φ_k) with $\theta_k = \arccos(k_z/k)$ and $\varphi_k = \arctan(k_y/k_x)$. When the origin is set at the sphere's center, the scattering field of an arbitrary beam is represented as[6,16]

$$p_s = \frac{1}{\pi}\sum_{n=0}^{\infty} i^n c_n h_n^{(1)}(kr) \sum_{m=-n}^{n} Y_{nm}(\theta,\varphi) \int\int_{k_x^2+k_y^2\le k^2} S(k_x,k_y)|_{z=z_s} Y_{nm}^*(\theta_k,\varphi_k) dk_x dk_y, \tag{3}$$

where c_n is the scattering coefficient of an isotropic elastic sphere,[23] $h_n^{(1)}$ is the spherical Hankel function of the first kind, the asterisk denotes the complex conjugate, and Y_{nm} are the normalized spherical harmonics[24] written as

$$Y_{nm}(\theta,\varphi) = \sqrt{\frac{(2n+1)(n-m)!}{4\pi(n+m)!}} P_n^m(\cos\theta) e^{im\phi}, \tag{4}$$

where P_n^m are the associated Legendre polynomials.

Based on the ASM, the simulation of acoustic scattering from the transducer array in Fig. 1 requires the angular spectrum $S(k_x, k_y)|_{z=z_s}$ at the sphere's location (x_s, y_s, z_s). Therefore, a planar scan is first performed on a near-field lateral plane (see Sec. 3.2). Then, the measured angular spectrum can be propagated to the target location via a transfer function (or the propagation factor[25])

$$S(k_x,k_y)|_{z=z_s} = S(k_x,k_y)|_{z=0} e^{ik_x x_s + ik_y y_s + i\sqrt{k^2-k_x^2-k_y^2}\, z_s}. \tag{5}$$

Note that the near-field scanning area is made as large as possible to include most of the acoustic energy from the source.[26] This helps capture more plane wave components from different directions and higher spatial frequency components of the angular spectrum. It is to acquire these components for accurate simulations of acoustic propagation and scattering.

3. Watertank experiments for finite-aperture vortex beam

3.1 Experiment setup and signal processing

Figure 1(a) illustrates the experimental configuration. In the water tank (0.5 m × 0.5 m × 1 m), a first-order vortex beam is produced by a self-fabricated transducer array and a scanning hydrophone is used to measure the acoustic pressure in a lateral plane. The transducer consists of 127 elements arranged in a hexagonal pattern within a circular aperture of the

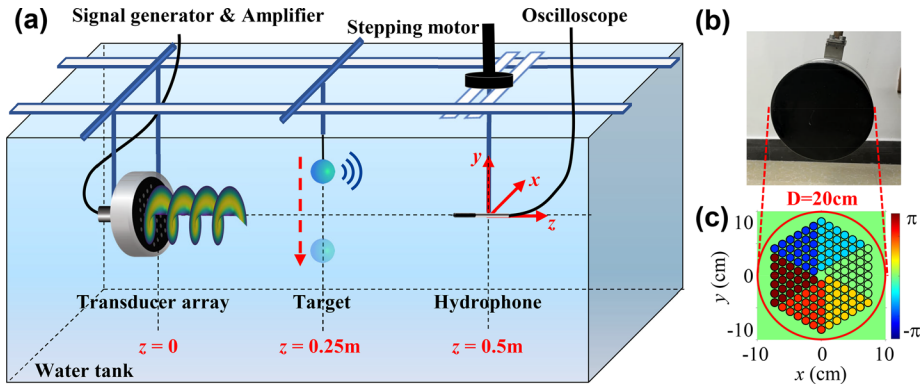

Fig. 1. (a) Schematic of the forward scattering experiment with a vortex beam transmitted from a transducer array and a scanning hydrophone acting as a planar receiver. The background (incident) field is first recorded. Subsequently, the lateral total fields in the forward direction are measured for the target (a PMMA sphere) moving across the beam axis with different offsets. (b) Photograph of the transducer array. (c) The initial phase distribution as the input of the array elements for generating a first-order vortex beam.

diameter D = 20 cm [Fig. 1(b)]. Each element has a diameter of 13 mm and a center-to-center spacing of 14 mm, driven by a ten-cycle tone burst at a central frequency $f = 70$ kHz. The sound speed measured in water at around 17 °C is approximately $c = 1450$ m/s, yielding a wavelength of $\lambda = 20.7$ mm. Phase modulation to generate a first-order acoustic vortex can be achieved in various ways, provided the initial phase exhibits angular dependence. To simplify experimental implementation, the array elements are grouped into six sectors for collective phase control, as shown in Fig. 1(c).

At the receiver plane ($z = 0.5$ m), a hydrophone scans in the xy plane on a uniform 50×50 grid over a 20×20 cm^2 area, with a step size of 0.4 cm ($\approx 1/5\,\lambda$). At each grid point, the received signal is processed via the Hilbert transform to construct the analytic signal, from which the complex pressure field is extracted. The time origin used for projection is defined as the central instant of the signal acquired at the central scan point. For simplicity, the measured voltage signal is used directly, as its normalized distribution is equivalent to that of the acoustic pressure.

The beam axis is first aligned by locating the maximum pressure position when the array operates without vortex phase modulation as coherent sources for a focused beam. With the transducer center defined as the origin, the coordinates of any point are precisely determined from the speed of sound in water. After recording the background vortex field (without a target), a PMMA sphere of radius $a = 2.1$ cm is placed at $z = 0.25$ m and translated along the y axis with a 5 mm-step from $y_s = 20$ mm to -20 mm. At each position, the forward scattering field is obtained by subtracting the background field from the recorded total measured field. The scattering process under the experimental conditions is numerically simulated using the ASM discussed in Sec. 2. For a PMMA sphere, the material parameters used are as follows: the density is 1190 kg/m^3, the speeds of longitudinal and shear waves are 2690 and 1340 m/s, respectively. The density of water is $\rho = 1000$ kg/m^3. Note that for consistency between experiments and simulation, particularly the phase results, it is important to ensure that the time-dependence factor (here, $e^{-i\omega t}$) is identical between the measurement system and ASM.

To extract the spatial phase distribution in the forward scattering field, a cross correlation method is employed[11] that yields a high correlation coefficient in regions of large phase gradient near the phase singularities. A unit normalization is applied to the complex pressure to avoid the influence of amplitude fluctuations. The phase factor is retained (i.e., $e^{i\phi}$) and correlated with a template matrix used to detect a rapid gradient. The template matrix is either extracted from a measurement centered on a singularity or simply constructed with a Laplacian operator. To precisely locate the phase singularity in the experimental correlation map, we apply the Whittaker–Shannon interpolation[26] for the measured fields to achieve the same computational resolution ($\approx 1/20\,\lambda$).

3.2 Measurement of the angular spectrum

According to Eq. (3), the angular spectrum covers all information of the incident field. In practice, we first measure the complex pressure in a near-field plane at $z = 0.12$ m and then propagate it numerically backward to reconstruct the source distribution $p_i(x, y, z = 0)$, as shown in Fig. 2(a). From the measurement, it can be observed that the phase structure of the acoustic vortex has already formed, and the low-amplitude region corresponding to the phase singularity is clearly visible. Since the array elements are divided into 6 sectors, distinct grating lobes appear encircling the phase singularity. In the backward projection, the transfer function is the conjugation of the forward version of Eq. (5). The scanning area here we used is a 25.2×25.2 cm^2 square with 64×64 points with the step size of 0.4 cm ($\approx 1/5\lambda$). After the backpropagation and the Whittaker–Shannon interpolation, the reconstructed source plane with a spatial resolution of $1/20\,\lambda$ clearly reveals the hexagonal pattern and the six sectors of the transducer array shown in Fig. 2(a).

The full incident field in the propagation plane is also displayed in Fig. 2(b) obtained from Eqs. (1) and (2). Figure 2(c) compares the directly measured and numerically reconstructed background field at the receiver plane

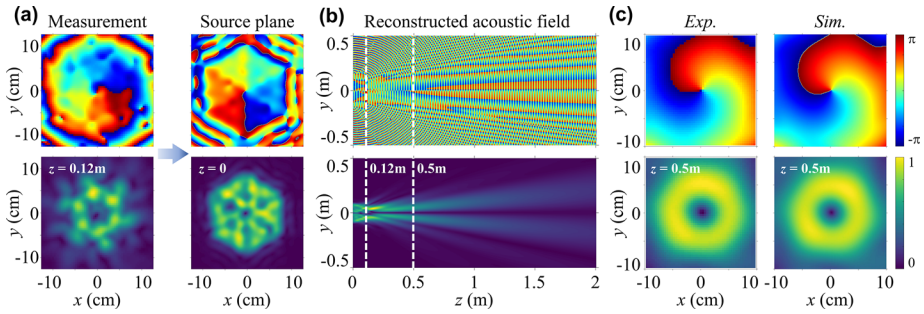

Fig. 2. (a) Reconstruction of the source field (i.e., the pressure phase in the upper right corner and amplitude in the lower right corner) from a near-field measurement at $z = 0.12$ m. (b) The pressure phase and amplitude in the propagation yz plane at the axial intervals of 1/2 λ in z direction. (c) Comparison of the pressure distribution at $z = 0.5$ m obtained from direct measurement and numerical simulation based on the ASM. The upper and lower panels display the phase and normalized amplitude, respectively.

($z = 0.5$ m), showing good agreement and thereby validating the accuracy of the extracted angular spectrum from our measuring system. Due to slight deviations in sound speed or distance, the phase distributions in the measured and simulated fields exhibit different rotational tendencies. To ensure consistency with the experimental phase reference which is the central time of the received wave train, a constant phase factor $e^{i2\pi/3}$ is applied to the complex pressure fields derived from ASM. Consequently, the field distributions shown in Fig. 2(c) are aligned well with the experimental reference without altering the phase structure. The same factor is similarly applied to subsequent calculations of acoustic scattering.

3.3 Experimental and simulation results

As shown in Fig. 3, the forward scattering results from simulations (upper half) and experiments (lower half) are presented. In each part, the rows from top to bottom correspond to the normalized amplitude, phase, and correlation coefficient scaled in dB, respectively. Different sphere offsets to the beam axis: $y_s = 20$, 10, 0, −10, and −20 mm are selected for Figs. 3(a)–3(e). It is shown that the phase distribution, particularly the phase singularity nearest the beam axis of the

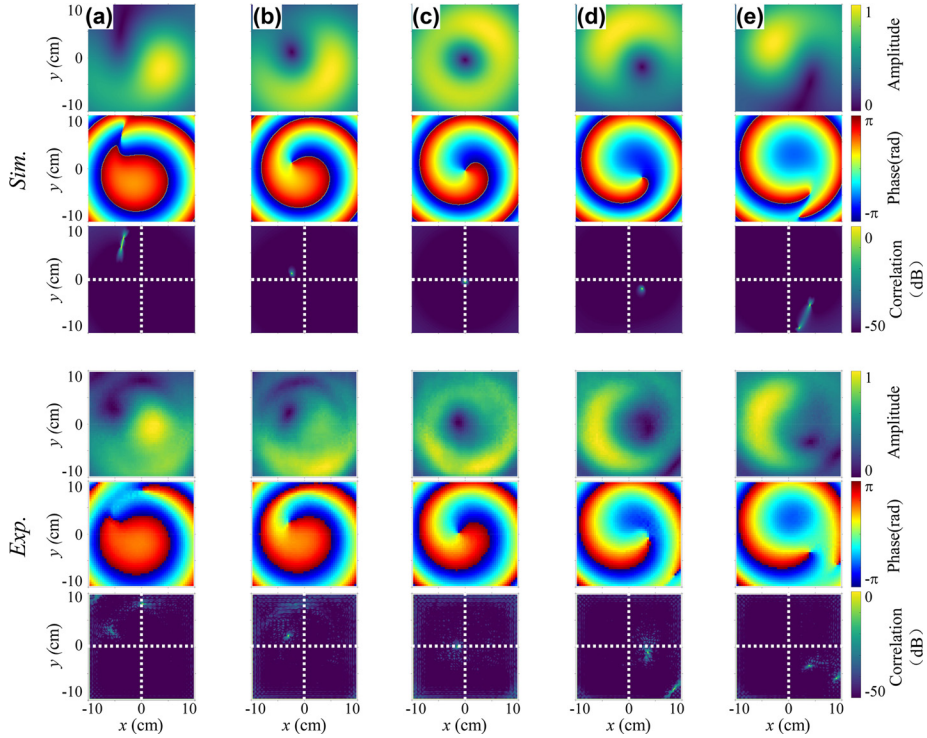

Fig. 3. Simulation and experiment results of the forward scattering field of a PMMA sphere located at (0, y_s, 0.25 m) with different positions: (a) y_s=20 mm, (b) y_s=10 mm, (c) y_s=0, (d) $y_s = -10$ mm, and (e) $y_s = -20$ mm. In either the simulation or experiments, the color plots show the normalized amplitude, phase, and correlation coefficients scaled in dB from the first to third rows, respectively. A movie is provided as supplementary material for the forward scattering field with different offsets.

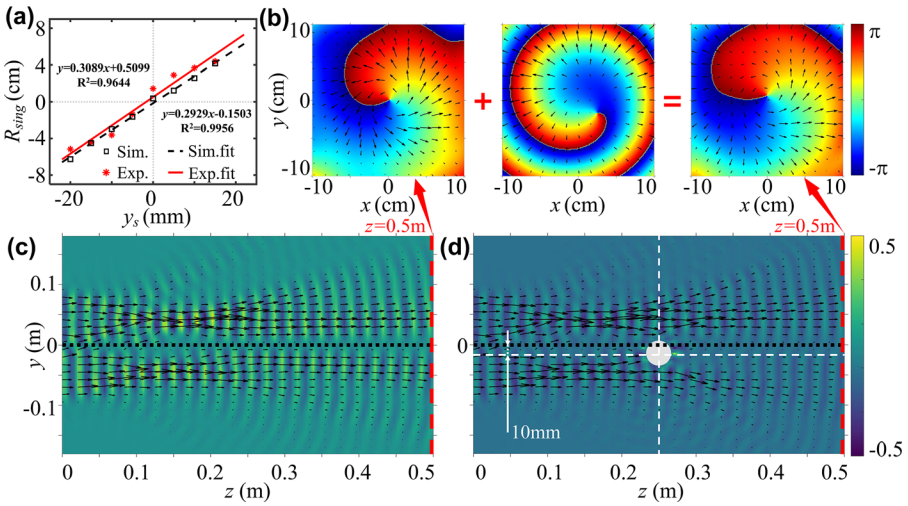

Fig. 4. (a) The shift distance of the phase singularity R_{sing} versus the sphere's offset to the beam axis y_s. The black and red symbols show the simulation and experiment results, respectively. (b) The total field (right-hand-side panel) contains the background (left-hand-side panel) and forward scattering (middle panel) components, where the arrows represent the transverse energy flux distribution in the xy plane at $z = 0.5$ m. The corresponding propagation yz plane features for the background and total field are also displayed in (c) and (d). The color plots in (b) show the lateral spatial phase, while in (c) and (d) show the normalized pressure amplitude.

pressure fields by simulations and experiments agree well. A phase singularity surrounded by a zero-amplitude area is present at the center of the forward scattering field[3] since the sphere preserves the symmetry of the vortex field for the on-axis case [see row (c) with $y_s = 0$], see Figs. 3(c). As the sphere moves off the beam axis, the broken symmetry causes the singularity shifting away from the center. The phase maps reveal that the phase singularity shifts as the sphere traverses the vortex field, and the direction of this shift depends on the relative spatial position between the target and the beam axis of the vortex. For equal but opposite target displacements, the results are expected to exhibit rotational symmetry. This phenomenon is confirmed by the present results [e.g., Figs. 3(b) and 3(d)]. In addition, as the offset increases, one more singularity emerges with a converse topological charge [Figs. 3(a) and 3(e)] in both experiments and simulation.

The features of this location-dependence of the phase singularity are well captured by the proposed cross correlation analysis. In the correlation maps, the phase singularity [marked as (x_{sing}, y_{sing})] corresponds to the location of the highest correlation coefficient, exceeding the background level by more than 50 dB. Subsequently, the shift distance $R_{sing} = \sqrt{x_{sing}^2 + y_{sing}^2}$ is extracted. For clarity, this distance is set to negative when the sphere position y_s is negative. Figure 4(a) plots the singularity shift as a linear function of the sphere position y_s. The R^2 values obtained from linear regression are 0.9644 for the experimental data and 0.9956 for the simulation, where R^2 denotes the square of the correlation coefficient between the observed data and the fitted line. This result provides a method for potential applications of target detection and identification induced by the interaction between vortex beams and an object.

To further depict the field disturbance, we calculate the transverse energy flux to characterize the incident and total field. For the scalar field ψ with $p = i\omega\rho\psi$, the energy flux $\mathbf{g} = \Im(\psi^* \nabla\psi)$ represents the direction of phase gradient of wave propagation.[27] The arrows of Fig. 4(b) show the transverse energy flux on the lateral spatial phase of the background (left), forward scattering (middle), and total fields (right) at $y_s = -10$ mm. Despite the influence of the scattered field, a phase singularity persists at the center of the total field, demonstrating the non-diffracting property of the vortex beam.[28] The energy flux in the scattered field propagates outward in a divergent pattern around the phase singularity. In the propagating plane, a zero-amplitude region progressively forms on the beam axis without a sphere inside [Fig. 4(a)] and the main acoustic energy propagates forward around the beam axis. However, a sphere alters the energy transport direction, particularly in the near-field [Fig. 4(b)], implying the disturbance of the vortex beam by the existing object.

4. Conclusions and discussions

In this work, we use the spatial phase as the degree of freedom to extract the forward scattering of a sphere in a vortex beam with both numerical simulations and experimental measurements. Note that the correlation analysis of the phase tuned by acoustic scattering or transmission is also used for imaging technologies such as the beamforming-focusing based echography and tomography, and the speckle correlation analysis is used for the Doppler in medical echography. Based on the proposed cross correlation method, the phase singularity is detected with a contrast exceeding 50 dB relative to the surrounding field. The linear relationship between singularity shift and target offset to the beam axis is obtained from experiments and validated through numerical simulation. Despite the realistic vortex beams are partly non-diffracting, the

implicit forward scattering still reveals the target position which may pave the way for the utilization of spatial phase in target detection and positioning. However, these results are obtained based on the assumption that the incident background should be stable. Once the background deviates from that of the measurement of the total scattering, this method may fail and is a challenge for further engineering application. As shown in Fig. 3, the method is efficient on the scattered field only since the total field and the incident field are nearly identical. In addition, the scattered wave is weak when the sphere is located inside the intensity ring of the vortex beam. This is because most of the acoustic energy is not illuminated on the target directly. The future work will explore the resolution limit of the proposed detection method and the potential prototype system in the field experiment which is not covered in the present work.

SUPPLEMENTARY MATERIAL

See the supplementary material for the forward scattering field with different offsets.

Acknowledgments

Z.G. thanks for the support from the National Natural Science Foundation of China (Grant Nos. 24Z990200542 and 12504522), the Joint Training Fund Project of Hanjiang National Laboratory (Grant No. LP2024004), the XIAOMI Foundation, and the Shanghai Jiao Tong University [2030 Initiative, AI for Engineering Initiative, and the startup funding (Grant Nos. WH220401017 and WH22040121)]. A Chinese patent (No. ZL 2024 1 0582905.8) and a U.S. patent (No. U.S. 12,510,661 B2) are related to this work.

AUTHOR DECLARATIONS

Conflict of Interest

The authors have no conflicts to disclose.

DATA AVAILABILITY

The data that support the findings of this study are available from the corresponding author upon reasonable request.

References

[1]J. Durnin, "Exact solutions for nondiffracting beams. I. The scalar theory," J. Opt. Soc. Am. A **4**(4), 651–654 (1987).
[2]J. Durnin, J. J. Miceli, and J. H. Eberly, "Diffraction-free beams," Phys. Rev. Lett. **58**(15), 1499–1501 (1987).
[3]P. L. Marston, "Scattering of a Bessel beam by a sphere: II. Helicoidal case and spherical shell example," J. Acoust. Soc. Am. **124**(5), 2905–2910 (2008).
[4]Z. Gong, P. L. Marston, W. Li, and Y. Chai, "Multipole expansion of acoustical Bessel beams with arbitrary order and location," J. Acoust. Soc. Am. **141**(6), EL574–EL578 (2017).
[5]M. Baudoin, J.-L. Thomas, R. A. Sahely, J.-C. Gerbedoen, Z. Gong, A. Sivery, O. B. Matar, N. Smagin, P. Favreau, and A. Vlandas, "Spatially selective manipulation of cells with single-beam acoustical tweezers," Nat. Commun. **11**(1), 4244 (2020).
[6]Z. Gong and M. Baudoin, "Equivalence between angular spectrum-based and multipole expansion-based formulas of the acoustic radiation force and torque," J. Acoust. Soc. Am. **149**(5), 3469–3482 (2021).
[7]C. Shi, M. Dubois, Y. Wang, and X. Zhang, "High-speed acoustic communication by multiplexing orbital angular momentum," Proc. Natl. Acad. Sci. U.S.A. **114**(28), 7250–7253 (2017).
[8]K. Wu, J.-J. Liu, Y-j Ding, W. Wang, B. Liang, and J.-C. Cheng, "Metamaterial-based real-time communication with high information density by multipath twisting of acoustic wave," Nat. Commun. **13**(1), 5171 (2022).
[9]B. T. Hefner and P. L. Marston, "An acoustical helicoidal wave transducer with applications for the alignment of ultrasonic and underwater systems," J. Acoust. Soc. Am. **106**(6), 3313–3316 (1999).
[10]P. L. Marston, "Phase and amplitude evolution of backscattering by a sphere scanned through an acoustic vortex beam: Measured helicity projections," J. Acoust. Soc. Am. **148**(2), EL135–EL140 (2020).
[11]T. Brunet, J.-L. Thomas, and R. Marchiano, "Transverse shift of helical beams and subdiffraction imaging," Phys. Rev. Lett. **105**, 034301 (2010).
[12]Y. Jia, Q. Hu, and S. Li, "Enhanced underwater three-dimensional imaging using acoustic orbital angular momentum waves and mode matching beamforming," J. Acoust. Soc. Am. **157**(2), 880–896 (2025).
[13]Z. Gong, L. Chen, J. Fan, B. Wang, F. Zhou, K. Zhao, J. Li, and Y. Yang, "Method for target detection based on correlation analysis of spatial phase in an acoustic vortex," U.S. patent 12,510,661B2 (December 30, 2025).
[14]P. L. Marston, "Scattering of a Bessel beam by a sphere," J. Acoust. Soc. Am. **121**(2), 753–758 (2007).
[15]D. Baresch, J.-L. Thomas, and R. Marchiano, "Three-dimensional acoustic radiation force on an arbitrarily located elastic sphere," J. Acoust. Soc. Am. **133**(1), 25–36 (2013).
[16]O. A. Sapozhnikov and M. R. Bailey, "Radiation force of an arbitrary acoustic beam on an elastic sphere in a fluid," J. Acoust. Soc. Am. **133**(2), 661–676 (2013).
[17]Z. Gong, W. Li, F. G. Mitri, Y. Chai, and Y. Zhao, "Arbitrary scattering of an acoustical Bessel beam by a rigid spheroid with large aspect-ratio," J. Sound Vib. **383**, 233–247 (2016).
[18]Z. Gong, P. L. Marston, and W. Li, "T-matrix evaluation of three-dimensional acoustic radiation forces on nonspherical objects in Bessel beams with arbitrary order and location," Phys. Rev. E **99**(6), 063004 (2019).
[19]M. Zampolli, F. B. Jensen, and A. Tesei, "Benchmark problems for acoustic scattering from elastic objects in the free field and near the seafloor," J. Acoust. Soc. Am. **125**(1), 89–98 (2009).

[20]V. Bollen, D. J. Zartman, T. M. Marston, and P. L. Marston, "Measured scattering of a first-order vortex beam by a sphere: Cross-helicity and helicity-neutral near-forward scattering and helicity modulation," Proc. Mtgs. Acoust. **19**, 070075 (2013).
[21]L. Ding, "Direct laboratory measurement of forward scattering by individual fish," J. Acoust. Soc. Am. **101**(6), 3398–3404 (1997).
[22]G. C. Gaunaurd and H. Überall, "Acoustics of finite beams," J. Acoust. Soc. Am. **63**(1), 5–16 (1978).
[23]G. C. Gaunaurd and H. Überall, "RST analysis of monostatic and bistatic acoustic echoes from an elastic sphere," J. Acoust. Soc. Am. **73**(1), 1–12 (1983).
[24]G. B. Arfken, H. J. Weber, and F. E. Harris, *Mathematical Methods for Physicists: A Comprehensive Guide*, 7th ed. (Academic Press, New York, 2012), pp. 756–757.
[25]Z. Gong and M. Baudoin, "Three-dimensional trapping and dynamic axial manipulation with frequency-tuned spiraling acoustical tweezers: A theoretical study," Phys. Rev. Appl. **16**(2), 024034 (2021).
[26]O. A. Sapozhnikov, S. A. Tsysar, V. A. Khokhlova, and W. Kreider, "Acoustic holography as a metrological tool for characterizing medical ultrasound sources and fields," J. Acoust. Soc. Am. **138**(3), 1515–1532 (2015).
[27]X.-D. Fan, Z. Zou, and L. Zhang, "Acoustic vortices in inhomogeneous media," Phys. Rev. Res. **1**(3), 032014 (2019).
[28]Z. Bouchal, J. Wagner, and M. Chlup, "Self-reconstruction of a distorted nondiffracting beam," Opt. Commun. **151**(4-6), 207–211 (1998).